J. Space Weather Space Clim. 2020, **10**, 24

https://doi.org/10.1051/swsc/2020024

JSWSC

Available online at:
www.swsc-journal.org

RESEARCH ARTICLE OPEN ACCESS

Very high energy proton peak flux model

Osku Raukunen[1,*], Miikka Paassilta[1], Rami Vainio[1], Juan V. Rodriguez[2], Timo Eronen[1], Norma Crosby[3], Mark Dierckxsens[3], Piers Jiggens[4], Daniel Heynderickx[5], and Ingmar Sandberg[6]

[1] Department of Physics and Astronomy, University of Turku, 20014 Turku, Finland
[2] Cooperative Institute for Research in Environmental Sciences (CIRES), University of Colorado, Boulder, 80309 CO, USA
[3] Royal Belgian Institute for Space Aeronomy (BIRA-IASB), Avenue Circulaire 3, 1180 Uccle, Belgium
[4] European Space Research and Technology Centre (ESTEC), Space Environment and Effects Section, Keplerlaan 1, 2200 AG Noordwijk, The Netherlands
[5] DH Consultancy, 3000 Leuven, Belgium
[6] Space Applications & Research Consultancy (SPARC), 105 51 Athens, Greece

Received 29 December 2019 / Accepted 26 May 2020

Abstract – Solar energetic particles (SEPs) pose a serious radiation hazard to spacecraft and astronauts. The highest energy SEPs are a significant threat even in heavily shielded applications. We present a new probabilistic model of very high energy differential peak proton fluxes. The model is based on GOES/HEPAD observations between 1986 and 2018, i.e., covering very nearly three complete solar cycles. The SEP event list for the model was defined using a statistical criterion derived by setting the possibility of false detection of an event to 1%. The peak flux distributions were calculated for the interpolated energies 405 MeV, 500 MeV and 620 MeV, and modelled with exponentially cut off power law functions. The HEPAD data were cleaned and corrected using a "bow-tie" method which is based on the response functions of the HEPAD channels P8–P10 found in the instrument calibration reports. The results of the model are available to the Space Weather community as a web-based tool at the ESA's Space Situational Awareness Programme Space Weather Service Network.

Keywords: Sun / energetic particle / modelling / particle radiation environment / space weather

1 Introduction

Solar energetic particles (SEPs) are an important component of the particle radiation environment in the space near Earth (Vainio et al., 2009). SEPs consist of protons, electrons and heavier nuclei. They arrive in bursts known as SEP events, which result from particle acceleration in flares in the solar corona and shocks associated with coronal mass ejections (CMEs). During SEP events the observed fluxes may increase by several orders of magnitude above the pre-event background. The events can last from a few hours to several days and their relative composition varies by many orders of magnitude from event to event. More details on SEPs can be found in reviews by e.g., Reames (1999, 2013) and Klein & Dalla (2017).

Particle radiation has harmful effects on both electronic equipment and biological organisms. Effects of energetic protons on electronics include single event effects (SEE) and solar cell degradation (e.g., Feynman & Gabriel, 1996; Fleetwood & Winokur, 2000; Iucci et al., 2005; Vainio et al., 2009, and references therein). SEE occur when particles deposit sufficient energy or charge in a sensitive region of a component, causing both non-permanent (soft) errors such as bit flips, and permanent (hard) errors such as latchups and burnouts (Dodd & Massengill, 2003; Sexton, 2003). Solar cells suffer from both total ionizing dose and displacement damage effects, resulting in reduced performance (Crabb, 1994; Gao et al., 2014). Biological organisms suffer from cellular damage caused by ionizing particle radiation. Effects of radiation in humans and animals can be categorized as deterministic (early) and stochastic (late) effects. Deterministic effects, such as cataracts, nausea, damage to internal organs, and even death, are caused by quick exposures to high doses of radiation, whereas stochastic effects, such as leukaemia and other types of cancer, are caused by longer exposures to lower dose rates (Facius & Reitz, 2007; Hellweg & Baumstark-Khan, 2007; Kennedy, 2014).

SEP events are an outcome of an extremely complex chain of physical processes, and their long-term deterministic prediction is currently practically impossible. Therefore, for space mission planning and instrument design, statistical models are needed to estimate the particle radiation environment in which the instruments and astronauts will need to survive the duration of the mission. The models are often based on SEP event flux

*Corresponding author: oajrau@utu.fi

distributions determined using long series of observations. The two most important quantities of SEPs in modelling are fluence (accumulated flux), related to degradation of electronic components and chronic biological radiation damage, and peak flux, related to SEE-induced error rates in electronics and acute biological radiation damage.

The first widely used proton fluence model was the King model (King, 1974), which used data from 1966 to 1972, making a separation between "ordinary" and "anomalously large" SEP events. Using an extended dataset and a continuous distribution of event fluences, Feynman et al. (1990) developed an updated version of the model which came to be known as the JPL model (Feynman et al., 1990, 1993, 2002). In this model the fluences at each integral energy threshold was modelled separately using lognormal distributions, and event occurrence was modelled as a Poisson process. Our modelling approach described in this article is similar to the JPL model, except for a different choice of distribution functions. Other examples of proton fluence models include the ESP and PSYCHIC models (Xapsos et al., 1999a, 1999b, 2000, 2004, 2007), which used the maximum entropy principle to obtain the distribution of event fluences (truncated power law) and the distribution of fluence accumulated over a mission (lognormal distribution); the MSU model (Nymmik, 1998, 1999, 2007), which modelled the shape of the fluence spectra and included a dependence on the solar activity; the SEPEM and SAPPHIRE models (Jiggens et al., 2012, 2018a, 2018b), in which the fluences were modelled with cut-off power law distributions and the event waiting times with a Lèvy distribution; and the two UTU models by Raukunen et al. (2018), one of which was based on a JPL-type approach and the other one an MSU-type approach.

For the estimation of peak fluxes there have not been so many options. A common practice has been based on a worst-case approach with a single well-known event like August 1972 (Adams et al., 1981) or October 1989 (Tylka et al., 1997), or a composite of events such as February 1956 and August 1972 (Anderson & Smith, 1994). The first probabilistic peak flux model was developed by Xapsos et al. (1998b) using the maximum entropy principle to obtain the initial distribution of the SEP event peak fluxes (a truncated power law) and extreme value theory (Xapsos et al., 1998a) to obtain the cumulative peak flux distributions for different mission durations. The model applies to >10 MeV protons during the seven active years of the solar cycle. The MSU model (Nymmik, 1999) based on distribution of spectral shapes, also includes peak flux estimation. In addition, the MSU model includes the whole solar cycle via a dependence of SEP event probability on sunspot number (an indicator of solar activity). More recently, the SEPEM model (Jiggens et al., 2012) and the subsequent SAPPHIRE model (Jiggens et al., 2018a, 2018b) included peak flux modelling. These models were based on a virtual timelines method which included event durations and their relation to peak fluxes and fluences.

Inside the Earth's magnetosphere, or in heavily shielded applications such as human spaceflight, the high energy part of the SEP spectrum becomes crucial. In addition to dose related effects, increased fluxes of high energy protons may cause dose rate related effects such as increased SEE rates in electronics (Petersen, 1996) and potentially dangerous acute radiation effects in astronauts (Parsons & Townsend, 2000; Hu et al., 2009). In this article, we present a new model of very high energy (405–620 MeV) 5 min and 1 h peak fluxes based on GOES/HEPAD observations between 1986 and 2017. The HEPADs' almost uninterrupted *in situ* observations present a unique, extremely long and homogenous dataset of very high energy protons. Of the previously published probabilistic SEP peak flux models only the MSU model has reached this energy range while being at least partly based on spacecraft observations (the >600 MeV channel on the Meteor satellites in some events; see Nymmik, 1999, and references therein). Other models have been either based on spectral extrapolations, or have not covered the energy range at all; therefore, our model provides a significant improvement to the current status of modelling.

The model presented in this paper has been released as an online tool as a part of the University of Turku's federated product (UTU-SEP) in the Space Radiation Expert Service Centre[1] (R-ESC) under the Space Weather (SWE) segment of the European Space Agency's (ESA's) Space Situational Awareness (SSA) programme. In addition to the peak flux model, UTU-SEP consists of a very high energy proton fluence model (Raukunen et al., 2018), a solar energetic proton event catalogue (Paassilta et al., 2017) and a high energy solar heavy ion fluence model. The SWE consists of four additional expert service centres: Solar Weather, Heliospheric Weather, Ionospheric Weather and Geomagnetic Conditions.

This article is structured as follows: in Section 2 we describe the GOES/HEPAD instrument and the data used in the study; in Section 3 we describe the SEP event list and the flux distributions used in our modelling; in Section 4 we discuss our results, and in Section 5 we present our conclusions. Further details on the "bow-tie" method of calculating HEPAD fluxes are given in Appendix.

2 Instruments and data

We have used proton flux observations of the High Energy Proton and Alpha Detector (HEPAD) (Onsager et al., 1996) onboard the Geostationary Operational Environmental Satellite (GOES) spacecraft operated by the National Oceanic and Atmospheric Administration (NOAA). The first GOES satellite was launched in October, 1975, and the most recent satellite (as of this writing), GOES-17, in March, 2018. A HEPAD flew on every GOES satellite from GOES-4 through GOES-15. The first ground-level enhancement (GLE) SEP event observed by a GOES HEPAD was GLE 39 (February 1984) and the most recent one was GLE 72 (September 2017). HEPAD consists of two silicon detectors and a Cherenkov detector, read-out with a photomultiplier tube (PMT), in a telescope configuration. It observes high energy protons in four energy channels above 350 MeV and alpha particles in two energy channels above 2560 MeV (Rinehart, 1978; Sellers & Hanser, 1996). We have used HEPAD data observed from the beginning of 1986 until the end of 2017, covering solar cycles 22 and 23 completely, and the vast majority of the current solar cycle 24. The data can be accessed online at NOAA's space weather satellite data services.[2]

[1] http://swe.ssa.esa.int/space-radiation
[2] https://www.ngdc.noaa.gov/stp/satellite/satdataservices.html

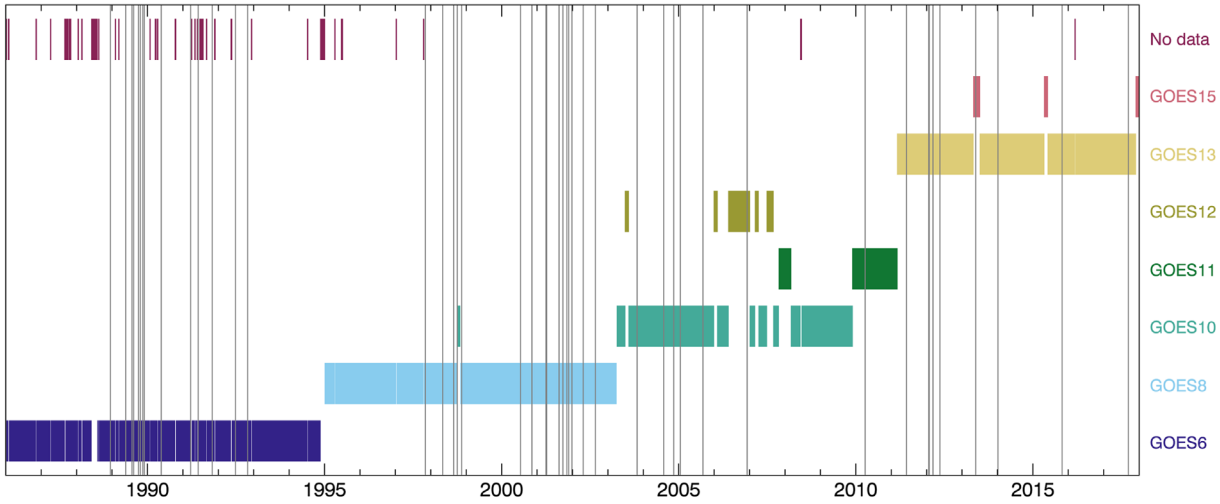

Fig. 1. Use of data from different GOES satellites over time shown (coloured horizontal bars), along with the SEP episodes (gray vertical lines).

Table 1. Nominal energy ranges and bow-tie energies of differential HEPAD channels P8–P10. Nominal energies taken from Panametrics, Inc. (1986) and Space Systems/Loral (1996).

Channel	1986–1994		1995→	
	Energy range (MeV)	Bow-tie energy (MeV)	Energy range (MeV)	Bow-tie energy (MeV)
P8	355–435	405	350–420	406
P9	435–555	473	420–510	457
P10	555–760	622	510–700	583

The use of data from different GOES missions in this study is shown schematically in Figure 1. The figure also shows the episodes of solar particle activity used in the modelling as gray vertical lines. The bulk of the data comes from GOES 6, 8, 10 and 13. GOES 11, 12 and 15 have been used to fill in gaps whenever possible. Some gaps in the data unfortunately still remain, mostly during the GOES-6 era when there were no overlapping HEPAD datasets. The periods with missing data are shown in the "no data" bars at the top of Figure 1.

In this study, we used the three differential HEPAD channels P8, P9 and P10. Since the channels are wide and their responses are heavily dependent on energy instead of being simple boxcar functions, the common practice of using the geometric mean energy to describe the channel may not be accurate. Therefore we perform a "bow-tie" analysis (see Appendix for details) to obtain more realistic effective energy values for each channel. The nominal energy ranges and the resulting bow-tie energies of the differential channels are given in Table 1. Channel P11 is an integral channel, and although it can be bow-tie-analysed as a differential channel, we did not use it in our model due to data issues which could not be explained by known uncertainties in the calibrations, and thus could not be solved within the scope of this study.

The 5 min averaged HEPAD data contain some "spikes", i.e., increases in flux of over an order of magnitude for individual datapoints. To clean the spikes, we compared the logarithm $\log_{10}(F_i)$ of each flux F_i with the median m of log-fluxes $\{\log_{10}(F_{i-6}), \ldots, \log_{10}(F_{i+6})\}$. Then, if $\log_{10}(F_i) > m + 1$, F_i was replaced with 10^m. In addition, we identified a few short periods of erroneous data after visual inspection and manually marked them as missing data. These periods are also included in the "no data" bars in Figure 1. None of the spikes or manually removed data coincide with SEP event onsets or peaks. After cleaning the 5 min flux time series, 1 h fluxes were calculated using moving averages, and both the 5 min and 1 h fluxes were inter/extrapolated to logarithmically spaced energies 405 MeV, 500 MeV and 620 MeV using linear fits in log–log-scales. In addition, a 30 min averaged dataset was created to be used in defining the SEP events that are used in the modelling.

3 Modelling

3.1 Event definition

As an event definition, we required that the flux $F^{30\ \mathrm{min}}$ must be higher than a threshold value F_{th} for a minimum of 6 h, i.e., for 12 consecutive 30-min datapoints. The threshold value was determined by requiring that the probability p_F of detecting a false event (purely by chance because of statistical fluctuation), should be equal to 0.01 over the complete dataset. Assuming there are enough counts in each time bin so that the fluxes are approximately normally distributed, it is known from probability theory that a single flux value exceeds F_{th} with probability p when they are related by the equation

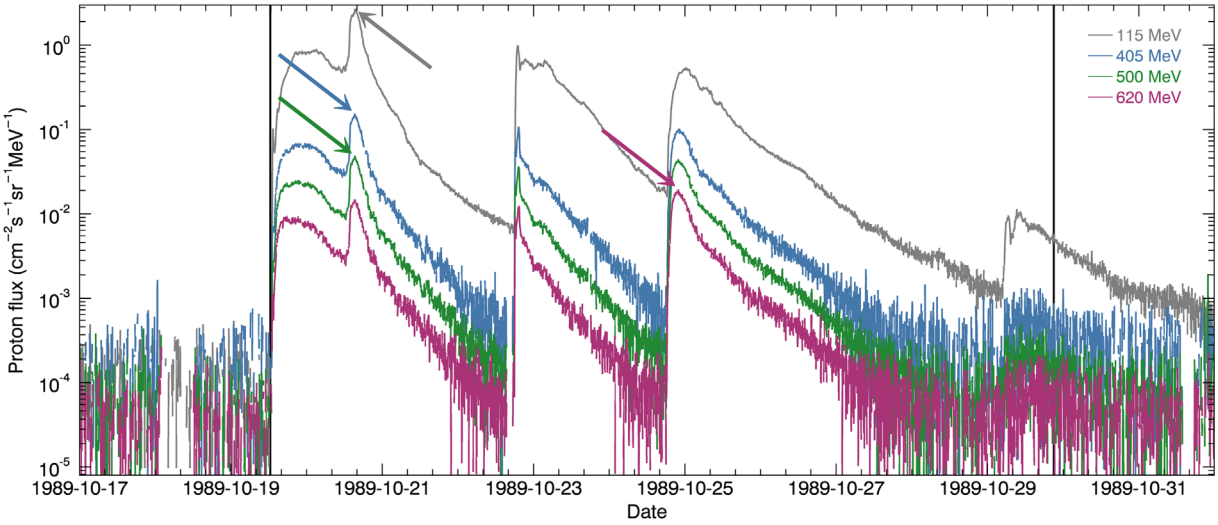

Fig. 2. The October 1989 solar energetic particle episode. HEPAD fluxes inter/extrapolated to 405 MeV, 500 MeV and 620 MeV are shown in blue, green and purple, respectively, and the 115 MeV SEPEM channel is shown in grey. The vertical lines show the onset and ending times of the episode. The arrows show the location of the maximum flux on each channel.

$$F_{\mathrm{th}} = \mu + \Phi^{-1}(1-p)\cdot\sigma, \tag{1}$$

where μ is the mean, σ is the standard deviation and Φ^{-1} is the quantile function. For 12 consecutive points the probability of exceeding is p^{12}. The value for p is defined using the probability limit for false event, i.e., $p^{12} = p_F/N = 0.01/N$, where N is the total number of datapoints in the three energy channels. This gives $p = 0.2068$, which further results in $\Phi^{-1}(1-p) = \Phi^{-1}(0.7932) = 0.8176$. Thus, we obtain the event criterion that the threshold flux $F_{\mathrm{th}} = \mu + 0.8176\sigma$ has to be exceeded continuously for at least 6 h. The μ and σ are calculated for each datapoint using the preceding 24 h, i.e., 48 datapoints, except for the 24 h after the end of a previous event, where μ and σ from before the event are used. When a flux value $F_i^{30\,\mathrm{min}}$ exceeds the threshold value, the μ and σ are fixed and the following points $F_{i+j}^{30\,\mathrm{min}}$ are compared to those values.

Based on this criterion, multiple SEP events may be interpreted as one, if the flux does not drop below the threshold between them, or one event may be split into multiple parts, if the flux happens to drop below the threshold during the event. The preliminary event lists, calculated separately for each channel, were combined into one event candidate list and cleaned in the following way. First, events that occurred at least partly simultaneously in different channels were combined into a single event candidate. For events that were detected in more than one channel, we selected the earliest onset time and the latest ending time. Then, we inspected the resulting list of event candidates visually to remove those events that were found only because of a Forbush decrease, or because of some data error, e.g., change in background caused by instrument change. Finally, we compared the list with previously published event lists (Papaioannou et al., 2016; Paassilta et al., 2017; Raukunen et al., 2018) and the NOAA X-ray flare list[3] to identify which solar active region was the most probable originator for each event candidate. All consecutive event candidates originating from the same active region were combined into episodes to ensure the statistical independence of their occurrence.

The final dataset consists of 46 independent SEP episodes, 22 of which include one or more GLEs. Of the 24 episodes that do not include GLEs, 20 include at least one "sub-GLE" listed in Vainio et al. (2017) and Raukunen et al. (2018). All GLEs occurring between 1989 and 2017 are included in the SEP episodes, except GLE 57 on 1998–05–06, which results in too small fluxes to be detected by our criterion. Figure 2 shows the October 1989 SEP episode, consisting of three large SEP events (GLEs 43–45) and a weak SEP event in the end of the episode. The HEPAD fluxes at 405 MeV, 500 MeV and 620 MeV are shown in blue, green and purple, respectively, and the 115 Me SEPEM channel (Jiggens et al., 2018a) is shown in grey for comparison. The black vertical lines show the onset and ending times of the episode. Note that a pre-event background has been subtracted from the fluxes (see Sect. 3.2 for details).

To find out if any SEP events were missed because of the HEPAD data gaps, we made a visual inspection of SEPEM channels over each >6 h period where HEPAD data is missing. There were seven events occurring completely or partially during a HEPAD data gap, but only one (on 1988–6–30) which had any visible flux increase in the two highest energy channels (166 MeV and 240 MeV) in SEPEM. However, these increases were small compared to increases in several other events that did not cause a detectable increase in HEPAD channels. Therefore, we can safely assume that none of the events occurring during a data gap would have been included in our event list.

Figure 3 shows the distribution of waiting times, i.e., times between the onsets of consecutive episodes. The black line shows an exponential fit to the waiting times under 1000 days, calculated as a linear fit to the logarithms of the waiting times. The fit describes the waiting times under 1000 days quite well, implying that their occurrence can be modelled as a Poisson process. Both of the waiting times greater than 1000 days occur

[3] ftp://ftp.ngdc.noaa.gov/STP/space-weather/solar-data/solar-features/solar-flares/x-rays/goes/xrs/

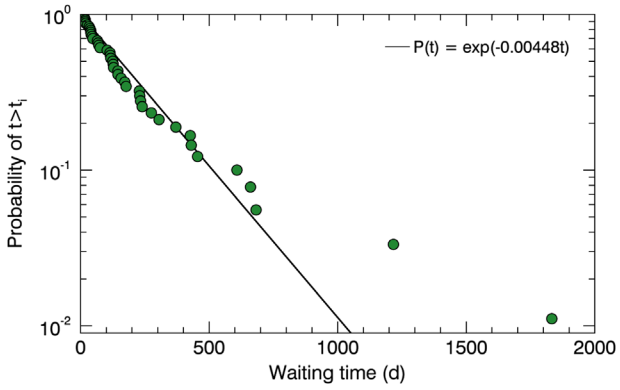

Fig. 3. Distribution of waiting times between SEP episodes and the exponential fit for waiting times under 1000 days.

between the last event of the previous cycle and the first event of the following cycle. Therefore, modelling the episode occurrence as a Poisson process is valid for the active part of the solar cycle, i.e., approximately from the beginning of the second year until the end of the eighth year of a solar cycle (Raukunen et al., 2018).

3.2 Flux distributions

To remove the contribution from galactic cosmic rays (GCRs), background subtraction was performed on the episode fluxes using the mean flux of the 24 h preceding each episode. In the cases where this background period started less than 10 days after the end of the previous episode, the background value for the previous episode was used. The peak fluxes for each episode were calculated simply as the maximae of the background-subtracted fluxes if each channel. This means that the episode peak fluxes in different channels may be found from different events inside the episode. An example of the peak definition is shown with the arrows in Figure 2, where the 405 MeV and 500 MeV peak fluxes are found at the shock peak after the first GLE on 1989–10–20 at 15:20 UTC, but the 620 MeV peak flux is found at the peak of the third GLE on 1989–10–24 at 21:55 UTC.

To be able to model the peak fluxes, we organize them by ascending size and assign a probability $P_i = (i - 0.5)/N$, where i is the rank of the flux and $N = 46$ is the total number of SEP episodes. This differs from the usual definition of empirical distribution function by the subtraction of 0.5; this way we obtain slightly larger fluxes for given probabilities, avoiding the implication that the largest flux in our observations would be at probability $P = 1$, that is, the largest possible flux. The resulting empirical cumulative distributions are shown in Figure 4, left panel for 5 min data and right panel for 1 h averaged data. We fitted the distributions with exponentially cut-off power law functions, i.e.,

$$F(\phi) = 1 - \frac{\phi^{-\gamma} \exp \frac{\phi_{\min}}{\phi_{\max}}}{\phi_{\min}^{-\gamma} \exp \frac{\phi}{\phi_{\max}}}, \quad (2)$$

where ϕ is the flux, γ is a power law index parameter and $\phi_{\min}$ and $\phi_{\max}$ are parameters that are related to the minimum and maximum flux of the distribution, respectively. The fits were calculated by minimizing the quantity:

$$\chi^2 = \sum_{i=23}^{46} \left((P_i - F(\phi_i))^2 \cdot \phi_i \right), \quad (3)$$

i.e., weighting the fit with the square root of the fluxes and only accounting for the points with $P > 0.5$. This is done to give enough weight to the highest-flux points, which are the most important since the range of interest for SEP modelling is usually above the 50% confidence level. Even though the fits overestimate the fluxes at probabilities below 50% by as much as a factor of three, it does not have an effect in the results at or above the 50% confidence level. The fits are shown as the coloured lines in Figure 4.

3.3 Modelling methodology

Our modelling follows the familiar JPL methodology (Feynman et al., 1990, 1993). First, the number of SEP episodes during a time period t is sampled from a Poisson distribution with parameter $\lambda = c_{wt} \cdot t$, where $c_{wt} = 0.00448$ d^{-1} = 1.636 a^{-1} is the fit parameter from the waiting time distribution from Figure 3. Then, for each episode, the peak fluxes are drawn, using rejection sampling, from the cut-off power law distributions determined in Section 3.2. Finally, the largest episode peak flux for each energy channel (or zero in the case of zero SEP episodes) is saved, and the whole process is repeated until a desired statistical accuracy is reached. In our modelling, we required that the relative standard errors (RSDs) of both 50th and 99th percentiles of the results were less than 1% between runs for all energy channels. The dependence of RSD on the number of repeats, N, was determined to be proportional to $C_t/\sqrt{N}$ for various values of $N < 20,000$ for different values of modelling time $0.5 \leq t \leq 7.0$ years. The required values for N were between 1.4×10^6 for $t = 0.5$ a and 1.8×10^5 for $t = 7.0$ a.

4 Results and discussion

As an example of the modelling results, Figure 5 shows the probability of exceeding a peak flux during 1 year and 7 year missions for 5 min and 1 h peak fluxes. Note that the curves do not start at $P = 1$ because there is a probability ($P_{k=0,t=1a} = 0.195$ and $P_{k=0,t=7a} < 0.001$) of having zero events and thus zero peak flux. Figure 6 shows the modelled peak flux as a function of energy for a two year mission at confidence levels 50% and 95%, i.e., the peak fluxes that are not exceeded with 50% and 95% probability, respectively. As a comparison, we show the results of an identical modelling (same event/episode list and functional form for the flux distributions) using a new version of the SEPEM reference dataset (Jiggens et al., 2012, 2018a), which includes data until December, 2017. Results for SEPEM channels 3–10 are shown with grey symbols.

There is a discrepancy between the HEPAD results and the highest energy SEPEM channels, especially at 95% confidence level. On the other hand, the HEPAD results and SEPEM channels 3–6 can be well fitted with a Band function, as shown by the blue lines in Figure 6. The Band function (Band et al., 1993) is a double power law function with a smooth exponential roll-over between the power laws, and is often used to describe SEP

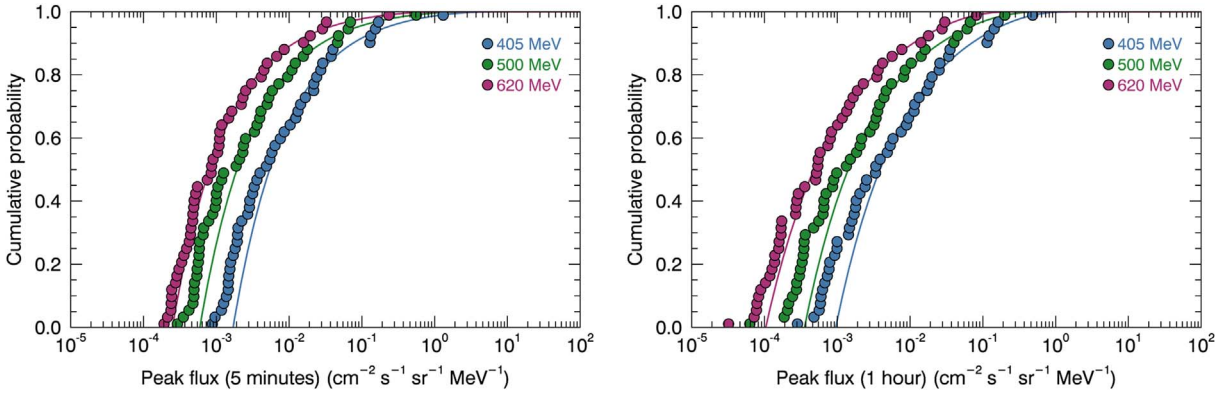

Fig. 4. Distribution of 5 min (left) and 1 h (right) peak fluxes of SEP episodes. The lines show the fitted cut-off power law functions.

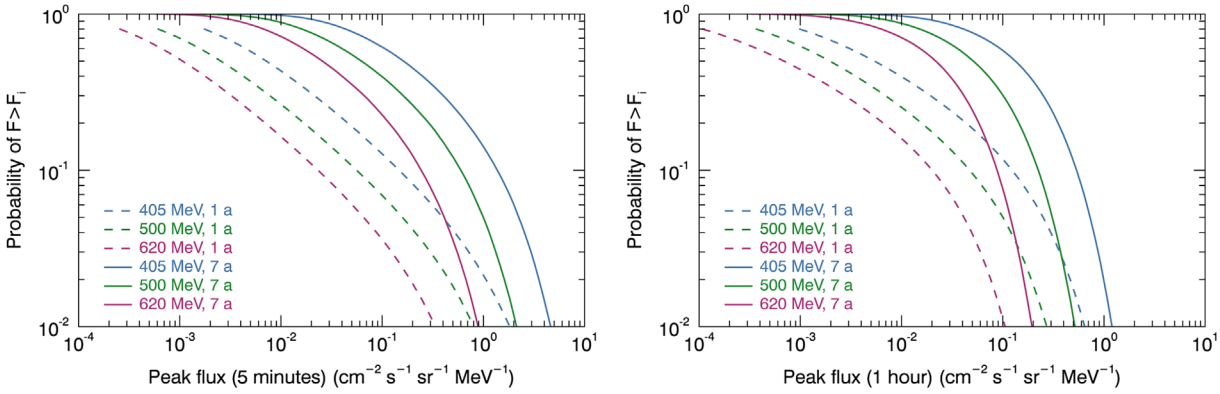

Fig. 5. The probability of exceeding a 5 min (left) and 1 h (right) peak flux for one year (dashed curve) and seven year (solid curve) missions.

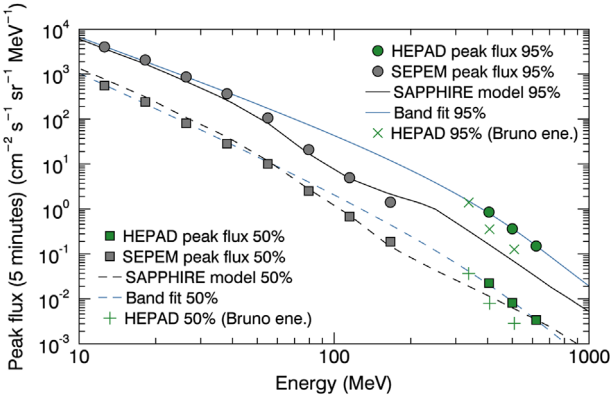

Fig. 6. Comparison of peak flux spectra for a two year mission at confidence levels 50% (squares) and 95% (circles). Green symbols show the results for HEPAD, grey symbols show the results for SEPEM data modeled similarly as the HEPAD data, and black lines show the results of the SAPPHIRE model. Blue lines show Band fits to HEPAD points and SEPEM points between 10 MeV and 50 MeV. Green plus signs and crosses show the HEPAD results converted to energies given by Bruno (2017); see the text for details.

spectra (e.g., Mewaldt et al., 2005; Tylka et al., 2005, 2006; Mewaldt et al., 2012; Zhao et al., 2016). The Band fit serves as a visual aid to show that even though the higher energy SEPEM channels disagree with the HEPAD results, the lower energy channels may agree. It should be noted that the shape of the model results, being obtained from a combination of different events at different energies, may not necessarily be well described by a Band function or other functional forms used to describe SEP event spectra.

In addition, corresponding results from the SAPPHIRE model (Jiggens et al., 2018a) are shown in Figure 6 as the black lines. SAPPHIRE is based on 5–289 MeV proton data observed by the Space Environment Monitors (SEM) onboard the SMS 1–2 and GOES 1–13 satellites. It is based on an entirely different modelling methodology and a much larger event list covering the active parts of solar cycles 21–24, whereas our model covers the solar cycles 22–24. The SAPPHIRE event list includes events that are not observed at higher energies, but depending on their spectra, may have much higher fluxes at lower energies. It is interesting to see that despite this, the SAPPHIRE model gives results quite close to the results of the SEPEM dataset modelled with our event list and methodology, even at lower energies. Our results are close to SAPPHIRE at 50% confidence level, but our spectrum is steeper. At 95% confidence level our results are higher by a factor of ~6. It should be noted, however, that above the 240 MeV channel, SAPPHIRE is not based on direct measurements, but a Band-fit extrapolation of the result spectra.

Figure 6 also shows our results converted to fluxes at energies defined for GOES-13 by Bruno (2017) (green plus signs

and crosses) by calibrating the HEPAD fluxes against fluxes observed by the PAMELA instrument (Adriani et al., 2014). Since our model results are based on the bow-tie fluxes whereas Bruno's results are based on nominal fluxes, we converted our results back to "nominal" values by multiplying with the bow-tie $G\Delta E$ and dividing with the nominal $G\Delta E$ (values for GOES-8 onwards, see Appendix). These values are somewhat closer to SAPPHIRE and the results for high energy SEPEM channels at 95% confidence level, but their spectra are steeper at both confidence levels (50% and 95%), which makes them slightly more incompatible with SAPPHIRE and SEPEM.

The apparent conservativeness, i.e., high predicted peak fluxes, of our model at higher confidence levels cannot be attributed to the modelling methodology (event selection, flux distribution fitting), since the SEPEM data were modelled with the same methods, yet it agrees with the SAPPHIRE results. Uncertainties in the bow-tie results (see Table A.1) are not sufficient to explain the differences between the results of the models. Therefore, they must be caused by differences in the original HEPAD and SEPEM data. Perhaps further studies, such as comparisons with SEP observations by space-based instruments such as PAMELA (Bruno et al., 2018) or AMS-02 (Bindi & AMS-02 Collaboration, 2015), or ground-based neutron monitors (e.g., Mishev et al., 2018), could provide insight into the matter. Modelling the response of the GOES particle instruments with GEANT4 (Allison et al., 2016), perhaps estimating the effect of the whole satellite structure, could also be beneficial in improving the results of the bow-tie analysis.

5 Conclusions

We have presented a new probabilistic model of very high energy solar energetic proton peak fluxes. The model is based on GOES/HEPAD data observed during 1986–2018. The data have been cleaned and corrected using a bow-tie analysis of the response functions, which is explained in Appendix. We model the SEP event occurrence as a Poisson process, and the peak flux distributions using exponentially cut-off power law functions. Comparison of our results with the SAPPHIRE model indicate that our model yields higher peak fluxes at high confidence levels, but is still spectrally compatible with the low energy part of SAPPHIRE. The model brings an important improvement to the current state of very high energy proton peak flux modelling. Online version of the model is available to the space weather community as part of ESA's Space Radiation Expert Service Centre.

Acknowledgements. The work at the University of Turku was conducted in the framework of the Finnish Centre of Excellence in Research of Sustainable Space, funded by the Academy of Finland (grant 312357). The research described in this paper was partly supported by ESA Contract 4000113187/15/D/MRP. We gratefully acknowledge the use of GOES data available online at NOAA NCEI Satellite Data Services. We also wish to acknowledge Paul Tol for the *muted qualitative* and *bright qualitative* colour maps (available at https://personal.sron.nl/~pault/) which we used in the figures throughout the article. The editor thanks two anonymous reviewers for their assistance in evaluating this paper.

References

Adams JH, Silberberg R, Tsao CH. 1981. Cosmic ray effects on microelectronics, part I: The near-earth particle environment. *Tech. Rep. NRL Memorandum Report 4506*, Washington, DC. URL https://apps.dtic.mil/dtic/tr/fulltext/u2/a103897.pdf.

Adriani O, Barbarino GC, Bazilevskaya GA, Bellotti R, Boezio M, et al. 2014. The PAMELA mission: Heralding a new era in precision cosmic ray physics. *Phys Rep* **544(4)**: 323–370. https://doi.org/10.1016/j.physrep.2014.06.003.

Allison J, Amako K, Apostolakis J, Arce P, Asai M, et al. 2016. Recent developments in GEANT4. *Nucl Instrum Methods Phys Res Sect A* **835**: 186–225. https://doi.org/10.1016/j.nima.2016.06.125.

Anderson BJ, Smith RE. 1994. Natural orbital environment definition guidelines for use in aerospace vehicle development. *Tech. Rep. NASA Technical Memorandum 4527*, Huntsville, AL. URL https://ntrs.nasa.gov/search.jsp?R=19940031668

Band D, Matteson J, Ford L, Schaefer B, Palmer D, et al. 1993. BATSE observations of gamma-ray burst spectra. I - Spectral diversity. *Astrophys J* **413**: 281–292. https://doi.org/10.1086/172995.

Bindi V, AMS-02 Collaboration. 2015. Solar energetic particles measured by AMS-02. In: *Proceedings of the 34th International Cosmic Ray Conference*, The Hague, The Netherlands. URL https://ui.adsabs.harvard.edu/abs/2015ICRC...34...10B.

Bruno A. 2017. Calibration of the GOES 13/15 high-energy proton detectors based on the PAMELA solar energetic particle observations. *Space Weather* **15(9)**: 1191–1202. https://doi.org/10.1002/2017SW001672.

Bruno A, Bazilevskaya GA, Boezio M, Christian ER, de Nolfo GA, et al. 2018. Solar energetic particle events observed by the PAMELA mission. *Astrophys J* **862(2)**: 97. https://doi.org/10.3847/1538-4357/aacc26.

Crabb RL. 1994. Solar cell radiation damage. *Radiat Phys Chem* **43(1)**: 93–103. https://doi.org/10.1016/0969-806X(94)90204-6.

Dodd PE, Massengill LW. 2003. Basic mechanisms and modeling of single-event upset in digital microelectronics. *IEEE Trans Nucl Sci* **50(3)**: 583–602. https://doi.org/10.1109/TNS.2003.813129.

Facius R, Reitz G. 2007. *Space weather impacts on space radiation protection, 289–352*, Springer, Berlin, Heidelberg. http://doi.org/10.1007/978-3-540-34578-7_11.

Feynman J, Gabriel S. 1996. High-energy charged particles in space at one astronomical unit. *IEEE Trans Nucl Sci* **43(2)**: 344–352. https://doi.org/10.1109/23.490754.

Feynman J, Armstrong TP, Dao-Gibner L, Silverman S. 1990. New interplanetary proton fluence model. *J Spacecr Rock.* **27**: 403–410. https://doi.org/10.2514/3.26157.

Feynman J, Spitale G, Wang J, Gabriel S. 1993. Interplanetary proton fluence model – JPL 1991. *J Geophys Res* **98**: 13. https://doi.org/10.1029/92JA02670.

Feynman J, Ruzmaikin A, Berdichevsky V. 2002. The JPL proton fluence model: an update. *J Atmos Sol-Terr Phys* **64(16)**: 1679–1686. https://doi.org/10.1016/S1364-6826(02)00118-9.

Fleetwood DM, Winokur PS. 2000. Radiation effects in the space telecommunications environment. In: *Proceedings of the 22nd International Conference on Microelectronics*, Vol. **1**, Niš, Serbia, pp. 43–49. https://doi.org/10.1109/ICMEL.2000.840529.

Gao X, Yang S, Feng Z. 2014. *Radiation effects of space solar cells*, Springer International Publishing, Cham, Switzerland, pp. 597–622. https://doi.org/10.1007/978-3-319-01988-8_20.

Hellweg CE, Baumstark-Khan C. 2007. Getting ready for the manned mission to Mars: the astronauts' risk from space radiation. *Naturwissenschaften* **94(7)**: 517–526. https://doi.org/10.1007/s00114-006-0204-0.

Hu S, Kim MY, McClellan GE, Cucinotta FA. 2009. Modeling the acute health effects of astronauts from exposure to large solar particle events. *Health Phys* **96(4)**: 465–476. https://doi.org/10.1097/01.HP.0000339020.92837.61.

Iucci N, Levitin AE, Belov AV, Eroshenko EA, Ptitsyna NG, Villoresi G, Chizhenkov GV, Dorman LI, Gromova LI, Parisi M. 2005. Space weather conditions and spacecraft anomalies in different orbits. *Space Weather* **3(1)**: S01,001. https://doi.org/10.1002/2003SW000056.

Jiggens PTA, Gabriel SB, Heynderickx D, Crosby N, Glover A, Hilgers A. 2012. ESA SEPEM project: Peak flux and fluence model. *IEEE Trans Nucl Sci* **59(4)**: 1066–1077. https://doi.org/10.1109/TNS.2012.2198242.

Jiggens P, Heynderickx D, Sandberg I, Truscott P, Raukunen O, Vainio R. 2018a. Updated model of the solar energetic proton environment in space. *J Space Weather Space Clim* **8**: A31. https://doi.org/10.1051/swsc/2018010.

Jiggens P, Varotsou A, Truscott P, Heynderickx D, Lei F, Evans H, Daly E. 2018b. The solar accumulated and peak proton and heavy ion radiation environment (SAPPHIRE) model. *IEEE Trans Nucl Sci* **65(2)**: 698–711. https://doi.org/10.1109/TNS.2017.2786581.

Kennedy AR. 2014. Biological effects of space radiation and development of effective countermeasures. *Life Sci Space Res* **1**: 10–43. https://doi.org/10.1016/j.lssr.2014.02.004.

King JH. 1974. Solar proton fluences for 1977–1983 space missions. *J Spacecr Rock.* **11**: 401. https://doi.org/10.2514/3.62088.

Klein K-L, Dalla S. 2017. Acceleration and propagation of solar energetic particles. *Space Sci Rev* **212(3)**: 1107–1136. https://doi.org/10.1007/s11214-017-0382-4.

Mewaldt RA, Cohen CMS, Labrador AW, Leske RA, Mason GM, Desai MI, Looper MD, Mazur JE, Selesnick RS, Haggerty DK. 2005. Proton, helium, and electron spectra during the large solar particle events of October–November 2003. *J Geophys Res* **110**: A09S18. https://doi.org/10.1029/2005JA011038.

Mewaldt RA, Looper MD, Cohen CMS, Haggerty DK, Labrador AW, Leske RA, Mason GM, Mazur JE, von Rosenvinge TT. 2012. Energy spectra, composition, and other properties of ground-level events during solar cycle 23. *Space Sci Rev* **171**: 97–120. https://doi.org/10.1007/s11214-012-9884-2.

Mishev A, Usoskin I, Raukunen O, Paassilta M, Valtonen E, Kocharov L, Vainio R. 2018. First analysis of ground-level enhancement (GLE) 72 on 10 September 2017: Spectral and anisotropy characteristics. *Sol Phys* **293(10)**: 136. https://doi.org/10.1007/s11207-018-1354-x.

Nymmik RA. 1998. Radiation environment induced by cosmic ray particle fluxes in the international space station orbit according to recent galactic and solar cosmic ray models. *Adv Space Res* **21**: 1689–1698. https://doi.org/10.1016/S0273-1177(98)00015-5.

Nymmik RA. 1999. Probabilistic model for fluences and peak fluxes of solar energetic particles. *Radiat Meas* **30(3)**: 287–296. https://doi.org/10.1016/S1350-4487(99)00065-7.

Nymmik RA. 2007. Improved environment radiation models. *Adv Space Res* **40(3)**: 313–320. https://doi.org/10.1016/j.asr.2006.12.028.

Onsager T, Grubb R, Kunches J, Matheson L, Speich D, Zwickl R, Sauer H. 1996. Operational uses of the GOES energetic particle detectors. In: *Proc. SPIE 2812, GOES-8 and Beyond*, Washwell ER (Ed.), pp. 281–290. https://doi.org/10.1117/12.254075.

Paassilta M, Raukunen O, Vainio R, Valtonen E, Papaioannou A, et al. 2017. Catalogue of 55–80 MeV solar proton events extending through solar cycles 23 and 24. *J Space Weather Space Clim* **7**: A14. https://doi.org/10.1051/swsc/2017013.

Panametrics, Inc. 1986. Report on the proton calibration of HEPADs SN6 and SN9 at the alternating gradient synchrotron of Brookhaven National Laboratory. *Tech. Rep. PANA-NOAA-CAL1*, 221 Crescent Street, Waltham, MA.

Panametrics, Inc. 1990. Report on the proton calibration of HEPAD SN 002 consisting of HEPAD: FAC PN 571774-01, serial no. 002 at the alternating gradient synchrotron of Brookhaven National Laboratory. *Tech. Rep. NXT-CAL-107*, 221 Crescent Street, Waltham, MA.

Papaioannou A, Sandberg I, Anastasiadis A, Kouloumvakos A, Georgoulis MK, Tziotziou K, Tsiropoula G, Jiggens P, Hilgers A. 2016. Solar flares, coronal mass ejections and solar energetic particle event characteristics. *J Space Weather Space Clim* **6(27)**: A42. https://doi.org/10.1051/swsc/2016035.

Parsons JL, Townsend LW. 2000. Interplanetary crew dose rates for the August 1972 solar particle event. *Radiat Res* **153(6)**: 729–733. https://doi.org/10.1667/0033-7587(2000)153[0729:ICDRFT]2.0.CO;2.

Petersen EL. 1996. Approaches to proton single-event rate calculations. *IEEE Trans Nucl Sci* **43(2)**: 496–504. https://doi.org/10.1109/23.490896.

Raukunen O, Vainio R, Tylka AJ, Dietrich WF, Jiggens P, Heynderickx D, Dierckxsens M, Crosby N, Ganse U, Siipola R. 2018. Two solar proton fluence models based on ground level enhancement observations. *J Space Weather Space Clim* **8**: A04. https://doi.org/10.1051/swsc/2017031.

Reames DV. 1999. Particle acceleration at the Sun and in the heliosphere. *Space Sci Rev* **90**: 413–491. https://doi.org/10.1023/A:1005105831781.

Reames DV. 2013. The two sources of solar energetic particles. *Space Sci Rev* **175**: 53–92. https://doi.org/10.1007/s11214-013-9958-9.

Rinehart MC. 1978. Cerenkov counter for spacecraft application. *Nucl Instrum Methods Phys Res Sect A* **154(2)**: 303–316. https://doi.org/10.1016/0029-554X(78)90414-7.

Sauer HH. 1993. GOES observations of energetic protons to E>685 MeV: Description and data comparison. In: *Proceedings of the 23rd International Cosmic Ray Conference*, Leahy DA, Hicks RB, Venkatesan D (Eds.), Vol. **3**, Calgary, Canada, pp. 250. URL https://ui.adsabs.harvard.edu/abs/1993ICRC....3..250S.

Sellers FB, Hanser FA. 1996. Design and calibration of the GOES-8 particle sensors: The EPS and HEPAD. In: *Proc. SPIE 2812, GOES-8 and Beyond*, Washwell ER (Ed.), pp. 353–364. https://doi.org/10.1117/12.254083.

Sexton FW. 2003. Destructive single-event effects in semiconductor devices and ICs. *IEEE Trans Nucl Sci* **50(3)**: 603–621. https://doi.org/10.1109/TNS.2003.813137.

Smart DF, Shea MA. 1999. Comment on the use of GOES solar proton data and spectra in solar proton dose calculations. *Radiat Meas* **30(3)**: 327–335. https://doi.org/10.1016/S1350-4487(99)00059-1.

Space Systems/Loral. 1996. GOES I-M DataBook. *Tech. Rep. DRL 101-08*.

Tylka AJ, Dietrich WF. 2009. A new and comprehensive analysis of proton spectra in Ground-Level Enhanced (GLE) solar particle events. In: *Proceedings of the 31st International Cosmic Ray Conference*, Giller M, Szabelski J (Eds.), Łódź, Poland. URL http://icrc2009.uni.lodz.pl/proc/pdf/icrc0273.pdf.

Tylka AJ, Adams JH, Boberg PR, Brownstein B, Dietrich WF, Flueckiger EO, Petersen EL, Shea MA, Smart DF, Smith EC. 1997. CREME96: A revision of the cosmic ray effects on micro-electronics code. *IEEE Trans Nucl Sci* **44(6)**: 2150–2160. https://doi.org/10.1109/23.659030.

Tylka AJ, Cohen CMS, Dietrich WF, Lee MA, Maclennan CG, Mewaldt RA, Ng CK, Reames DV. 2005. Shock geometry, seed populations, and the origin of variable elemental composition at

high energies in large gradual solar particle events. *Astrophys J* **625**: 474–495. https://doi.org/10.1086/429384.

Tylka AJ, Cohen CMS, Dietrich WF, Lee MA, Maclennan CG, Mewaldt RA, Ng CK, Reames DV. 2006. A comparative study of ion characteristics in the large gradual solar energetic particle events of 2002 April 21 and 2002 August 24. *Astrophys J Suppl Ser* **164(2)**: 536–551. https://doi.org/10.1086/503203.

Vainio R, Desorgher L, Heynderickx D, Storini M, Flückiger E, et al. 2009. Dynamics of the Earth's particle radiation environment. *Space Sci Rev* **147**: 187–231. https://doi.org/10.1007/s11214-009-9496-7.

Vainio R, Raukunen O, Tylka AJ, Dietrich WF, Afanasiev A. 2017. Why is solar cycle 24 an inefficient producer of high-energy particle events? *Astron Astrophys* **604**: A47. https://doi.org/10.1051/0004-6361/201730547.

Van Allen JA, Baker DN, Randall BA, Sentman DD. 1974. The magnetosphere of Jupiter as observed with Pioneer 10: 1. Instrument and principal findings. *J Geophys Res* **79(25)**: 3559. https://doi.org/10.1029/JA079i025p03559.

Xapsos MA, Summers GP, Burke EA. 1998a. Extreme value analysis of solar energetic proton peak fluxes. *Sol Phys* **183(1)**: 157–164. https://doi.org/10.1023/A:1005075421711.

Xapsos MA, Summers GP, Burke EA. 1998b. Probability model for peak fluxes of solar proton events. *IEEE Trans Nucl Sci* **45(6)**: 2948–2953. https://doi.org/10.1109/23.736551.

Xapsos MA, Barth JL, Stassinopoulos EG, Burke EA, Gee GB. 1999a. Space environment effects: Model for emission of solar protons (ESP): Cumulative and worst case event fluences. *Tech. Rep*. URL https://ui.adsabs.harvard.edu/abs/1999STIN...0021507X.

Xapsos MA, Summers GP, Barth JL, Stassinopoulos EG, Burke EA. 1999b. Probability model for worst case solar proton event fluences. *IEEE Trans Nucl Sci* **46(6)**: 1481–1485. https://doi.org/10.1109/23.819111.

Xapsos MA, Summers GP, Barth JL, Stassinopoulos EG, Burke EA. 2000. Probability model for cumulative solar proton event fluences. *IEEE Trans Nucl Sci* **47(3)**: 486–490. https://doi.org/10.1109/23.856469.

Xapsos MA, Stauffer C, Gee GB, Barth JL, Stassinopoulos EG, McGuire RE. 2004. Model for solar proton risk assessment. *IEEE Trans Nucl Sci* **51(6)**: 3394–3398. https://doi.org/10.1109/TNS.2004.839159.

Xapsos MA, Stauffer C, Jordan T, Barth JL, Mewaldt RA. 2007. Model for cumulative solar heavy ion energy and linear energy transfer spectra. *IEEE Trans Nucl Sci* **54(6)**: 1985–1989. https://doi.org/10.1109/TNS.2007.910850.

Zhao L, Zhang M, Rassoul HK. 2016. Double power laws in the event-integrated solar energetic particle spectrum. *Astrophys J* **821(1)**: 62. https://doi.org/10.3847/0004-637X/821/1/62.

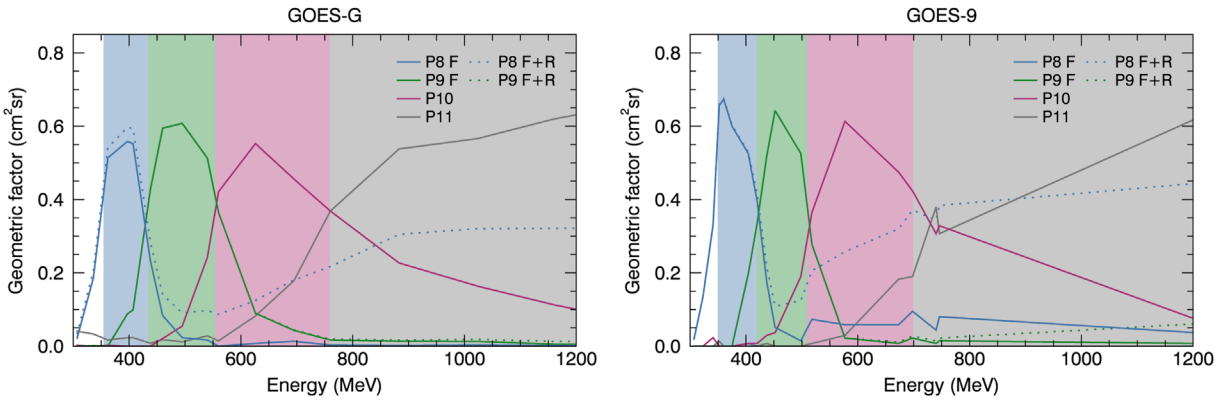

Fig. A.1. Energy dependence of geometric factor of HEPAD channels P8–P11 for GOES-G (left) and GOES-9 (right). The solid lines show the geometric factor for front entry particles, and the dashed lines show the geometric factor for both front and rear entry particles (rear entry only significant for P8 and P9). The background colors show the nominal energy ranges of the channels.

Appendix

Bow-tie analysis of HEPAD channels

This appendix describes a comprehensive bowtie analysis of the HEPAD proton channel energy responses as measured in an energetic proton beam. The HEPAD units are referred to by the names of the GOES satellites on which they flew.

The observed counting rate R of a particle detector can be given as integral of the product of the true differential flux $j(E)$ and the (energy-dependent) geometric factor of the detector $G(E)$, i.e.,

$$R = \int_0^\infty j(E)G(E)\mathrm{d}E. \tag{A.1}$$

For a detector consisting of a number of narrow energy channels with boxcar-like geometric factors, this can be approximated for each channel as

$$R = j(E_{\mathrm{eff}})G\Delta E, \tag{A.2}$$

where $j(E_{\mathrm{eff}})$ is the true flux at the effective channel energy E_{eff}, G is the channel's geometric factor and ΔE is the channel width. E_{eff} is usually defined as the geometric mean of the channel, which is correct for a boxcar geometric factor and a power law spectrum with power law index -2. The true flux at the effective channel energy can then be obtained from equation (A.2). For a wide channel with an energy-dependent geometric factor, unfolding the true flux spectrum $j(E)$ from the measured counting rate becomes ambiguous since there may be different $j(E)$ resulting in the same counting rate. On the other hand, estimating E_{eff} and $G\Delta E$ may be difficult without prior knowledge of $j(E)$.

The energy dependence of the geometric factors of the HEPAD channels for front entry particles according to reports of calibrations in a proton beam at Brookhaven National Laboratory (Panametrics, Inc., 1986, 1990) are shown with the solid lines in Figure A.1 for GOES-G (left) and GOES-9 (right). The dashed lines show the sum of front and rear entry particles for channels P8 and P9; for P10 and P11 the effect of rear entry is insignificant. The background colors correspond to the nominal energy ranges of channels P8–P11. Note that several different values for the channel ranges are given in the literature (e.g., Rinehart, 1978; Panametrics, Inc., 1986; Sauer, 1993; Sellers & Hanser, 1996; Space Systems/Loral, 1996; Smart & Shea, 1999); the figure shows the values given in (Panametrics, Inc., 1986) for GOES-G and in (Space Systems/Loral, 1996) for GOES-9. The HEPADs on GOES-G[4] and GOES-9 are the only calibrated units. GOES-G was built in the same group as GOES-4–7, so we use the calibrated GOES-G geometric factor for GOES-6. GOES-9, on the other hand, was built in the same group as the other units in the GOES-8–12 series, and we use its calibration for the whole series. Since none of the GOES-13–15 units are calibrated, we use the GOES-9 calibration for them also.

As Figure A.1 shows, the HEPAD geometric factors vary inside the nominal channel ranges, and some channels have a significant response outside the nominal range, and therefore it is difficult to estimate E_{eff} and $G\Delta E$ without knowing the spectrum $j(E)$ beforehand. To find suitable values, we solve for $G\Delta E$ from equation (A.2) and input R from equation (A.1) to get

$$G\Delta E = \frac{\int_0^\infty j(E)G(E)\mathrm{d}E}{j(E_{\mathrm{eff}})}. \tag{A.3}$$

We can assume the flux spectrum to be a power law of energy, i.e. $j(E) \propto E^{-\gamma}$, resulting in

$$G\Delta E = \frac{\int_0^\infty E^{-\gamma}G(E)\mathrm{d}E}{E_{\mathrm{eff}}^{-\gamma}}. \tag{A.4}$$

The channels can be analysed similarly as integral channels, yielding

$$G_I(E_t) = \frac{\int_0^\infty E^{-\gamma}G(E)\mathrm{d}E}{\int_{E_t}^\infty E^{-\gamma}\mathrm{d}E}. \tag{A.5}$$

[4] The rocket on which the GOES-G satellite rode exploded shortly after launch.

Table A.1. Results of bow-tie analysis for differential channels.

Channel (differential)	GOES-6		GOES-8→	
	E_{eff} (MeV)	$G\Delta E$ (cm^2 sr MeV)	E_{eff} (MeV)	$G\Delta E$ (cm^2 sr MeV)
P8FR	405	93.2 (−8.1%, +21.7%)	406	110 (−8.2%, +22.4%)
P9FR	473	84.5 (−2.2%, +6.3%)	457	66.3 (−1.8%, +5.2%)
P10	622	135 (−4.1%, +11.7%)	583	136 (−4.3%, +12.3%)
P11	780	199 (−10.1%, +31.5%)	775	149 (−5.6%, +16.0%)

Table A.2. Results of bow-tie analysis for integral channels.

Channel (integral)	GOES-6		GOES-8→	
	E_t (MeV)	G (cm^2 sr)	E_t (MeV)	G (cm^2 sr)
P8FR + P9FR + P10 + P11	350	0.833 (−2.3%, +5.9%)	345	0.872 (−2.0%, +4.9%)
P8FR + P9FR + P10	336	0.650 (−1.7%, +1.8%)	337	0.747 (−0.5%, +0.6%)
P9FR + P10 + P11	422	0.705 (−0.9%, +2.1%)	411	0.662 (−0.5%, +1.2%)
P9FR + P10	395	0.461 (−8.0%, +4.3%)	392	0.483 (−5.6%, +2.7%)
P10	486	0.303 (−7.4%, +3.6%)	462	0.352 (−4.3%, +2.2%)
P10 + P11	530	0.652 (−1.5%, +3.6%)	494	0.603 (−1.1%, +2.8%)
P11	623	0.404 (−5.4%, +13.9%)	640	0.373 (−2.2%, +5.6%)

Table A.3. Nominal $G\Delta E$ values used in GOES data processing.

Channel	GOES-6	GOES-8→
	$G\Delta E$ (cm^2 sr MeV)	$G\Delta E$ (cm^2 sr MeV)
P8	77.0	67.5
P9	48.0	67.5
P10	369	162
P11	1310	1565

By varying the power law index γ we obtain a family of effective-energy-dependent curves for $G\Delta E$, which converge in the middle, forming a "bow-tie"-like diagram, originally named by Van Allen et al. (1974). The convergence point gives the most optimal values for E_{eff} and $G\Delta E$ for the range of power law spectra used in the analysis. The point is found by minimizing the difference in 95th and 5th percentiles of values of $G\Delta E$. The range of power law indices was [1.9, 8.9], based on the range of proton power laws observed in GLEs (Tylka & Dietrich, 2009).

The results of the bow-tie analysis are given in Tables A.1 and A.2 for differential and integral channels, respectively. Table A.3 lists the $G\Delta E$ values used to calculate the fluxes available at https://www.ngdc.noaa.gov/stp/satellite/satdataservices.html. To convert those fluxes to bow-tie fluxes, they need to be first converted into counting rates by multiplying them with the correct nominal $G\Delta E$ from Table A.3, and then divided with the correct bow-tie $G\Delta E$ values from Table A.1. In the case of integral fluxes, the counting rates are summed (HEPAD counting rates can be summed because they are logically mutually exclusive) before dividing with appropriate bow-tie G values from Table A.2. Note that the integral channel P11 has been processed as a differential channel in the data files, which is why the nominal $G\Delta E$ value is given in differential units in Table A.3. It is important to remember that the range of spectral indices used to calculate the bow-tie values is valid for SEPs, but not GCRs; therefore, background subtraction should always be performed when using the bow-tie fluxes.

Cite this article as: Raukunen O, Paassilta M, Vainio R, Rodriguez JV, Eronen T, et al. 2020. Very high energy proton peak flux model. *J. Space Weather Space Clim.* **10**, 24.